

Bimodal substrate biasing to control γ - Al_2O_3 deposition during reactive magnetron sputtering

Marina Prenzel,^{1, a)} Annika Kortmann,¹ Adrian Stein,¹ Achim von Keudell,¹ Farwah Nahif,² and Jochen M. Schneider²

¹⁾*Research Group Reactive Plasmas, Ruhr-Universität Bochum, D-44801 Bochum, Germany*

²⁾*Materials Chemistry, RWTH Aachen University, D-52074 Aachen, Germany*

Al_2O_3 thin films have been deposited at substrate temperatures between 500°C to 600°C by reactive magnetron sputtering using an additional arbitrary substrate bias to tailor the energy distribution of the incident ions. The films were characterized by X-ray diffraction (XRD) and Fourier transform infrared spectroscopy (FTIR). The film structure being amorphous, nanocrystalline, or crystalline was correlated with characteristic ion energy distributions. The evolving crystalline structure is connected with different levels of displacements per atom (dpa) in the growing film as being derived from TRIM simulations. The boundary between the formation of crystalline films and amorphous or nanocrystalline films was at 0.9 dpa for a substrate temperature of 500°C. This threshold shifts to 0.6 dpa for films grown at 550°C.

^{a)}Electronic mail: marina.prenzel@rub.de

I. INTRODUCTION

Reactive magnetron sputtering (RMS) is a prominent technique to deposit many thin film materials as for examples oxides and nitrides using metal targets and the addition of oxygen and/or nitrogen as a reactive component to the argon plasma gas¹⁻⁴. The film stoichiometry and its structure can be adjusted by controlling the ion-to-neutral ratio in the film forming growth flux and the energy of the incident ions given by the ion energy distribution function (IED). Incident ions may enhance the adatom mobility and promote thereby crystallinity and/or a certain crystalline orientation^{3,5,6}. This is often quantified by the energy per deposited atom $\langle E \rangle$. This energy depends on the ion energy E_{ions} and on the ion-to-neutral ratio J_{ions}/J_{growth} in the growth flux with $\langle E \rangle = E_{ions} \cdot j_{ions}/j_{growth}$. Here, j_{ions} is the flux of incident ions and j_{growth} the total flux of incorporated atoms in the film.

Under variation of the average parameter $\langle E \rangle$ and the ion to neutral ratio j_{ions}/j_{growth} , it was shown by Adibe *et al.*⁷ and Petrov *et al.*⁸ that the average energy per incorporated atom $\langle E \rangle$ is no universal parameter for the formation of titanium nitride (Ti_{0.5}Al_{0.5}N). However, in addition to Musil *et al.*⁹, the average energy per incorporated atom is suggested to define the formation of crystallinity by several authors¹⁰⁻¹².

Recently, we devised an experiment to very accurately control the growth flux and the energy distribution of the incident ions¹³ by keeping the average energy per deposited atom $\langle E \rangle$, the average energy of the incident ions $\langle E_{ions} \rangle$, the total ion flux j_{ions} and the ion-to-neutral ratio j_{ions}/j_{growth} constant, but changing *only* the ion energy distribution (IED), for details see¹³.

We applied this concept to RMS of Al₂O₃ films as a prominent material with applications ranging from microelectronics, wear resistant coatings to catalytic surfaces⁴. The most common phases of Al₂O₃ are the γ - and α -phase. α -Al₂O₃ with its hexagonal closed package (hcp)¹⁴ structure is often used as hard coating on machining tools.

In 2005 Rosen *et al.* have reviewed phase formation data reported for vapor phase deposited alumina⁶ and summarize that the majority of authors observe that the crystalline growth temperature appears to be reduced as the mobility of surface species through energetic ion bombardment is increased. In 2010 Jiang *et al.* report an alpha alumina formation temperature of 560°C by utilizing large ion fluxes during PACVD¹⁵ as discharge power densities of 19 Wcm⁻² resulted in an increase in the energy and the flux of the bombarding

species towards the growing film, as well as in a more efficient precursor dissociation¹⁵. In the same year, Sarakinos *et al.* reported an alpha alumina formation temperature of 720°C by cathodic arc deposition¹⁶ for substrate bias potentials between -40 V and -200 V. Based on ab initio molecular dynamics calculations¹⁷ subplantation of the impinging Al is identified to cause significantly larger irradiation damage and hence larger mobility in the gamma alumina as compared to alpha alumina. Consequently, the enhanced mobility results in the growth of the alpha phases at the expense of the gamma phase.

From the above discussion it can be learned that in addition to the well-established mechanism of ion bombardment mediated surface diffusion the previously overlooked subplantation mechanism^{16,17} was suggested to be relevant for the formation of crystalline alumina thin films.

Previously¹³, we monitored the transition from X-ray amorphous to γ -alumina to assess the influence of the ion energy distribution on thin film growth, indicating that typically one displacement per incorporated atom (dpa) is necessary for that transition to occur. In this paper, we expand the data set and measured a comprehensive set of XRD and FTIR data to also identify nanocrystalline samples, which appear as being crystalline in the FTIR measurement although they are still X-ray amorphous. Based on this large data set, the hypothesis of characteristic dpa levels to allow for a certain structural transitions in the films can be more thoroughly tested. Formation of amorphous films, of nanocrystalline films or of X-ray γ -crystalline Al_2O_3 films was observed by FTIR and XRD. It has to be emphasized that our parameter interval is restricted to only the variation of the ion energy distribution function of the incoming ions and the substrate temperature. Therefore, it is possible to isolate the effect of the transfer of kinetic energy on the film growth.

II. EXPERIMENTAL METHODS

A. Film deposition

Thin aluminum oxide films were deposited using a dual frequency magnetron sputter experiment employing 13.56 MHz and 71 MHz for plasma generation, as described in detail in¹³. The discharge was operated at 0.1 Pa at a constant argon flow rate of 9 sccm. The base pressure in the deposition chamber was $2 \cdot 10^{-5}$ Pa. Based on^{13,18} this is expected to lead to H incorporation of $<2\text{at.}\%$. The incorporated H atoms from water in the residual gas¹⁹ is small enough that the effect of incorporated water in the films can be neglected. A feedback loop regulated the oxygen flow into the chamber to avoid target poisoning by monitoring a constant intensity of the Al I emission line at 396.2 nm using a narrow band pass filter and a photomultiplier. The adjusted oxygen partial pressure in the deposition chamber was determined as $8.6 \cdot 10^{-3}$ Pa in average. Thereby, stoichiometric Al_2O_3 coatings were prepared as being verified by ex-situ X-ray Photoelectron Spectroscopy (XPS).

The distance between target and the p-doped Si(100) substrate was 50 mm. The substrate temperature during the deposition process was regulated to 500 °C, 550 °C and 600 °C, respectively. The substrate temperature was directly measured by analyzing the temperature dependent refraction index of silicon at 632.8 nm by ellipsometry²⁰. This is non intrusive and measures directly the surface temperature. Any thermocouple at the substrate holder may read a different temperature due to improper thermal contacts. Pyrometry remain ambiguous because the emissivity of the coated silicon wafer is not well defined and silicon becomes transparent in the infrared wavelength range at high temperatures.

B. Substrate biasing and ion energy distribution

The substrate electrode was intentionally biased to tailor the ion energy distribution function (IEDF) of the incident ions. Rectangular waveforms were generated by a waveform generator and amplified using a broadband amplifier. A coupling capacitor was used to connect the biasing signal to the substrate electrode.

The kinetic energy of the impinging ions is controlled as follows: a rectangular biasing signal can be divided into an on-time (τ_{on}) and an off-time (τ_{off}). The frequency of the pulsing f is given as $f = 1/(\tau_{on} + \tau_{off})$. In our experiments, the on-time τ_{on} was fixed to

a value of 500 ns and a change in frequency f of the applied biasing signal was realized by changing the off-time τ_{off} only. Thereby, the fluence ($= j_{ions}\tau_{on}$) of energetic ions during growth remains identical in all experiments. The maximum ion energy $E_{ions,max}$, in case of collisionless sheaths, corresponds to the voltage drop between the biasing signal U_{max} and the plasma potential. Consequently, $E_{ions,max}$ was used as parameter to uniquely characterize the ion bombardment during film growth.

A typical bias signal for a frequency $f=1.01$ MHz and a maximum voltage of $U_{max} = -110$ V is shown in Figure 1 (a) as being measured at the substrate electrode by an oscilloscope. The signal is not perfectly rectangular due to the low pass filtering effect of the coupling capacitor. The resulting IEDF was simulated from the voltage signal at the electrode by a sheath model, as described by Shihab *et al.*²¹. The resulting IEDF is shown in Figure 1 (b) as ion flux per ion energy interval versus ion energy.

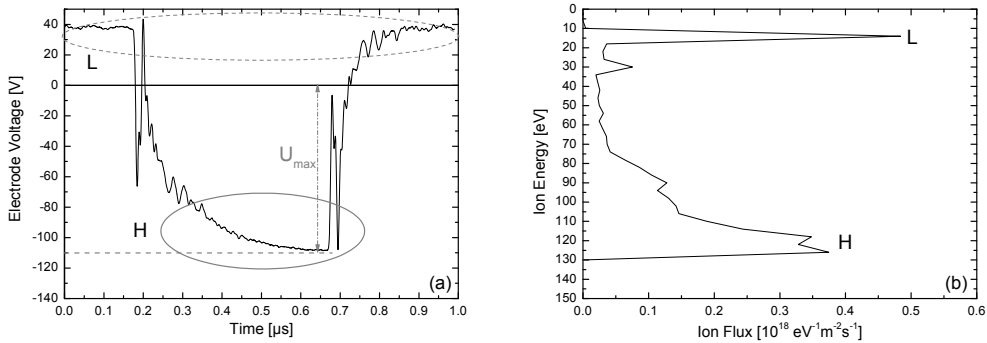


FIG. 1. (a) Rectangular biasing signal at the substrate electrode at 1.01 MHz, as measured by the oscilloscope. (b) simulated ion energy distribution function IEDF for the given bias signal by the model from Shihab *et al.*²¹. L and H indicate the low and high energy part of the IEDF, respectively.

Two prominent peaks (regions H and L in Figure 1) in the IEDF can be identified. The maximum ion energy $E_{ions,max}$ within the IEDF in Figure 1 (b) corresponds to the maximum bias voltage applied to the substrate electrode U_{max} (region H). During this time period, ions are accelerated by the voltage drop between plasma potential (18 V) and maximum bias voltage to the substrate electrode (U_{max}). This results in a maximum ion energy of $E_{ions,max} = 18 eV - U_{max} \cdot e$. In addition, a low energetic peak (region L) originates from ions accelerated during the off-time τ_{off} with an ion energy corresponding to the voltage drop between plasma potential and floating potential.

Frequencies f between 0.80 MHz and 1.60 MHz were applied to regulate the ratio between the ion flux at high vs. low ion energies. The ion energy of the high energetic peak within the IEDF was adjusted to a desired ion energy by a defined tailoring of the maximum bias voltage U_{max} . Therefore, any ratio between the two peaks within the IEDF and any position of the high energetic peak can be reached by tailoring frequency f and maximum bias voltage U_{max} .

The energy impact during film growth is usually defined by the mean energy per incorporated atom $\langle E \rangle$ depending on the maximum ion energy of the ions $E_{ions,max}$, the total growth flux j_{growth} , the ion flux j_{ions} and the duty cycle $d.c. = \tau_{on} \cdot f$ according to:

$$\langle E \rangle = E_{ions,max} \cdot \frac{j_{ions}}{j_{growth}} \cdot \tau_{on} \cdot f \quad (1)$$

The growth flux j_{growth} is defined by the incorporated flux of aluminum and oxygen atoms during Al_2O_3 film formation. This is deduced from the total film thickness, as measured ex situ by a profilometer, divided by the overall deposition time. The growth rate g expressed in $nm\ s^{-1}$ is converted into the growth flux in $cm^{-2}s^{-1}$ using the density of the film ρ and the average mass M of Al_2O_3 via $j_{growth} = \frac{g \cdot \rho}{M}$. A residual thickness inhomogeneity of 4% is observed which converts into an error of the growth flux of 5%.

Because XRD analysis of our films exhibits good crystalline quality of γ -alumina (see below), the film density value from literature of $\rho=3.66\ g \cdot cm^{-3}$ as being reported by Levin *et al.*²² seems to have reasonable good agreement with our films and is taken for the further discussion.

Finally, the ion flux to the substrate surface is required when determining the mean ion energy per incorporated atom $\langle E \rangle$. The ion flux j_{ions} was measured using a retarding field analyzer within a previous work²³. It was determined as $j_{ions}=13.5 \cdot 10^{18}\ m^{-2}s^{-1}$.

C. Thin film analysis

Phase formation was studied by XRD with a Bruker D8 General Area Diffraction System (GADDS) on the deposited Al_2O_3 thin films. The incident angle of the beam was 15° and the analyzed 2θ angle range was 20° to 75° . The applied voltage and current settings were 40 kV and 40 mA, respectively. Three different peaks which can be associated to the γ phase of Al_2O_3 are identified in the diffraction patterns of our samples. The (311) direction can be

found within the XRD pattern at an angle of 37.30° . Moreover, peaks at 45.86° and 67.03° are identified as (400) and (440) orientations, respectively. Peak positions agree with the JCDPS file number 10-0425 for γ - Al_2O_3 at 45.9° and 67.0° .

Further analysis of the Al_2O_3 samples was realized by ex situ FTIR transmission measurements using a Bruker IFS 66/S spectrometer. A polarizer was placed in front of the sample, so that only s polarized light reached the sample. The angle of incidence normal to the surface was 60° . Measurements were performed in the wavenumber range between 400 cm^{-1} and $6,000\text{ cm}^{-1}$. Background spectra of non-coated silicon wafers were used.

Brüesch *et al.*²⁴ investigated FTIR spectra of amorphous and γ -aluminum oxide. The evolution of a sharp peak (or dip within transmission spectra) at 950 cm^{-1} is characteristic for γ - Al_2O_3 . Further broad oscillations at lower wavenumbers being characterized by Chu *et al.*²⁵ at 357 cm^{-1} , 536 cm^{-1} and 744 cm^{-1} were identified.

XRD and FTIR assess the crystallinity of the samples on distinct length scales: (i) in XRD, the coherent scattering of the incident X-radiation from a crystal leads to pronounced peaks in the XRD diffractogram. In case of nanocrystalline samples, significant line broadening occurs which complicates the evaluation of X-ray profiles. As a consequence, the distinction between crystalline and amorphous samples depends on the employed diagnostic method and nanocrystalline samples may not be detected by XRD. (ii) in FTIR, the signal originates from the absorption of single Al-O bonds at a frequency depending on the configuration of the next neighbors. If nanocrystallites are formed, characteristic LO or TO phonon peaks may appear in the infrared spectrum, whereas the coherent overlap of the scattered light in XRD by crystalline region and amorphous sites may still show X-ray amorphous diffraction patterns.

Based on the different measurement principles of XRD and FTIR, the transition from amorphous, nanocrystalline, to crystalline samples can be assessed, as illustrated in Figure 2 for films deposited at different deposition conditions, as described below: (i) Figure 2 show the spectra for amorphous films, since no distinct peaks in the XRD diffractogram (a) and no sharp absorption for TO phonon at approximately 950 cm^{-1} is found (b) ; (ii) Figure 2 shows an XRD diffractogram (c) for a nanocrystalline film, which appears XRD-amorphous. Infrared absorption at a wavenumber of 950 cm^{-1} reflects the formation of nanocrystallites, which is shown in Figure 2 (d); (iii) Figure 2 shows an XRD diffractogram (e) for a crystalline film with sharp peaks in the XRD diffractogram at position characteristic to γ -alumina. In

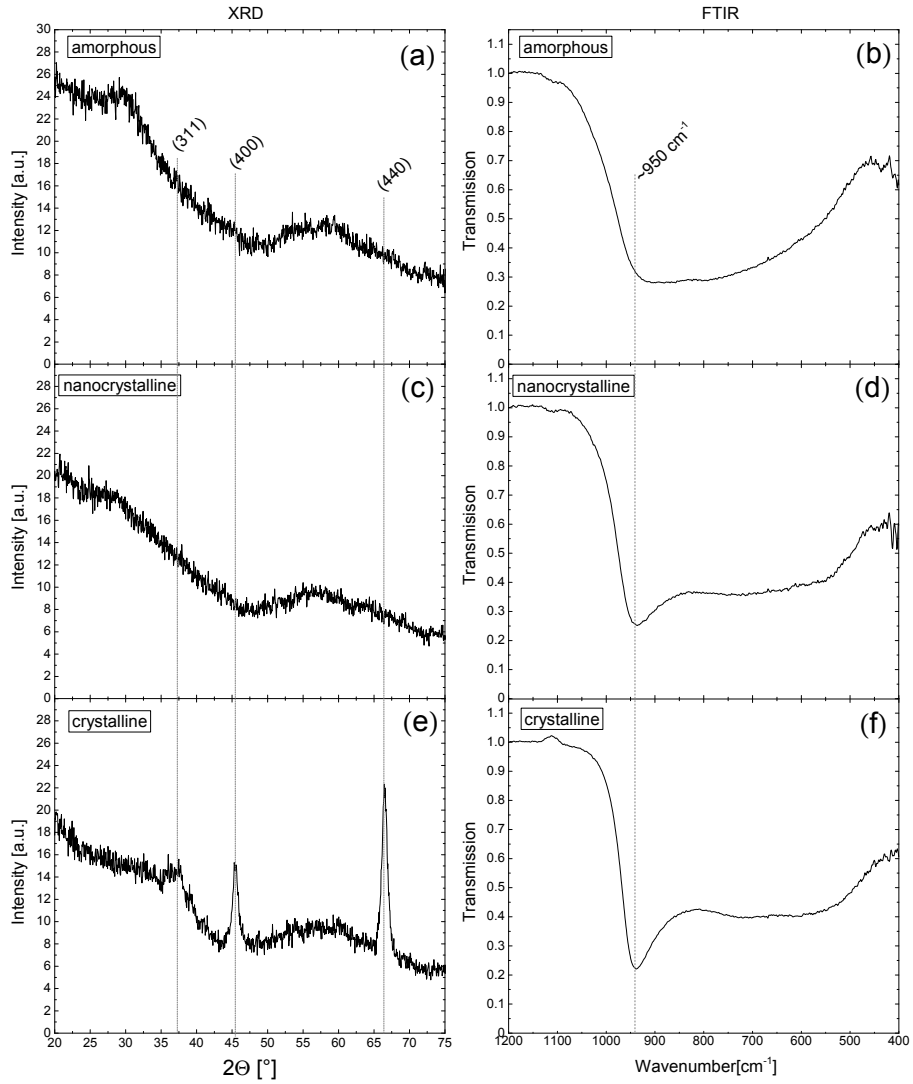


FIG. 2. Typical XRD- and FTIR-spectra for amorphous samples (a and b), for nanocrystalline samples (c and d), and for crystalline samples (e and f).

addition to the XRD signature, pronounced absorptions for TO phonon become also visible in the IR spectrum (f).

It is important to note that the identification of the nanocrystalline phase from a comparison of the XRD and FTIR data remains ambiguous for very few cases, because the sharpness of the TO-phonon peak in FTIR is not as distinct as the analysis of the diffraction peaks in the XRD diffractogram. Those samples are marked in the presented data sets.

III. RESULTS AND DISCUSSION

A large set of 73 samples was prepared in the substrate temperature range between 500 ° and 600 °C at a pressure of 0.1 Pa. The IEDF was tailored using frequencies f in the range between 0.80 MHz and 1.60 MHz for the pulsed bias and maximum bias voltages between -25 V to -280 V. The range of operating parameters and the resulting average energies $\langle E \rangle$ are listed in Table I. The samples were analyzed ex situ by XRD and FTIR with respect to their structure. The deposition is characterized by the maximum ion energy $E_{ions,max}$ and the average energy per incorporated atom $\langle E \rangle$. Figure 4 shows the results for the amorphous samples (open triangle), the nanocrystalline samples (half filled squares), and the crystalline samples (solid squares) for three different substrate temperatures of 500 °C (Figure 4a), of 550 °C (Figure 4b), and of 600 °C (Figure 4c). The dashed areas in Figure 4 indicate deposition parameters, which are not reasonable, because the average energy $\langle E \rangle$ cannot be larger than the maximum energy $E_{ions,max}$.

Finally, the correlation of the deposition parameters with the structure of the deposited films may be affected by nucleation phenomena.

Deposition/ Biasing parameter	Adjusted values
Temperature T	500 °C, 550 °C, 600 °C
Biasing frequency f	0.80 MHz, 1.01 MHz, 1.20 MHz, 1.40 MHz, 1.60 MHz
Mean energy per incorporated atom $\langle E \rangle$	10 eV...30 eV...60 eV
Maximum Biasing voltage U_{max}	-25 V...-280 V
Maximum ion energy $E_{ions,max}$	7 eV...262 eV

TABLE I. Deposition parameters for Al₂O₃ growth by reactive magnetron sputtering with an additional substrate bias.

The data in Figure 4 indicate that crystalline films are usually obtained if the average energy $\langle E \rangle$ and the maximum energy $E_{ions,max}$ are above a certain threshold. This becomes more critical at lower substrate temperatures, where also amorphous films are observed at low $\langle E \rangle$ and $E_{ions,max}$. The films at intermediate values for $\langle E \rangle$ and $E_{ions,max}$ show nanocrystalline behavior. At a temperature of 600 °C, aluminum oxide is deposited in the γ phase even for very low ion bombardment and only very few samples remain amorphous.

This rough analysis already illustrates that an increasing energy input during film growth induces a transition of the film structure from an amorphous to a nanocrystalline and finally to a crystalline structure. This is in agreement with the current general understanding of energetic film deposition.

The ion-induced formation of a nanometer size crystal or the γ phase could be induced by displacement events within a collision cascade. These displacements generate mobility and may turn enable the the formation of a crystalline structure. This very general picture can be tested with our data by comparing the samples, as plotted in Figure 4, with TRIM simulations²⁶ to calculate the displacements per incorporated atoms in the growing films.

TRIM simulations were performed for argon ions, which initiate a collision cascade in an stoichiometric Al_2O_3 film. Surface binding energies for Al atoms and O were assumed as 3.36 eV and 2.00 eV, respectively. A density of 3.66 g cm^{-3} was assumed²² and mono energetic argon ions with energies between 28 eV and 308 eV. This corresponds to maximum voltages at the substrate electrode U_{max} of -10 V to -300 V, respectively. The displacement per ion (dpi) for the different ion energies was calculated and plotted versus ion energy in Figure 3. No distinction between displacing aluminum or oxygen is made. A threshold energy of 32 eV for aluminum oxide is necessary to induce a displacement event within the Al_2O_3 film. Ion bombardment by a rectangular bias signal establishes two distinct peaks with different ion energies impinging onto the substrate surface. Ions with low energies with 18 eV are below the threshold to initiate a displacement within the aluminum oxide film. Only ions with ion energies above the critical value of 32 eV have enough energy to initiate a displacement within the film. The low energetic ions are accelerated within the off period of the bias signal, whereas high energetic ions are produced during the on-time of the signal. Therefore, only ions from the high energetic peak within the IEDF account to the dpi within the Al_2O_3 films.

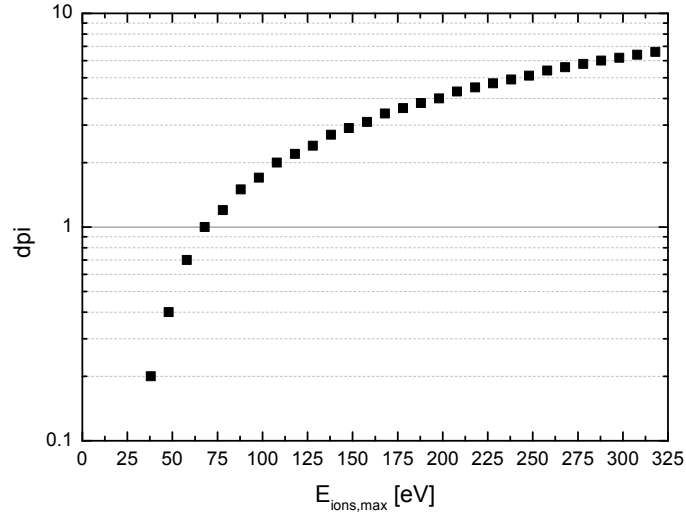


FIG. 3. TRIM calculation for displacement per ion (dpi) for Ar ions impinging onto an Al_2O_3 surface.

The displacements per ion (dpi) are converted into displacements per atom (dpa) during film growth by multiplying it with the ratio between energetic ion fluence per puls $\dot{j}_{ions}\tau_{on}$ and the growth fluence $\dot{j}_{growth}(\tau_{on} + \tau_{off})$:

$$dpa = dpi \cdot \frac{\dot{j}_{ions}}{\dot{j}_{growth}} \frac{t_{on}}{t_{on} + t_{off}} = dpi \cdot \frac{\dot{j}_{ions}}{\dot{j}_{growth}} t_{on} \cdot f \quad (2)$$

Equation 1 can be combined with eq. 2 yielding a dependence of the dpa level on the control parameters $E_{ions,max}$ and $\langle E \rangle$:

$$dpa = dpi \cdot \frac{\langle E \rangle}{E_{ions,max}} \quad (3)$$

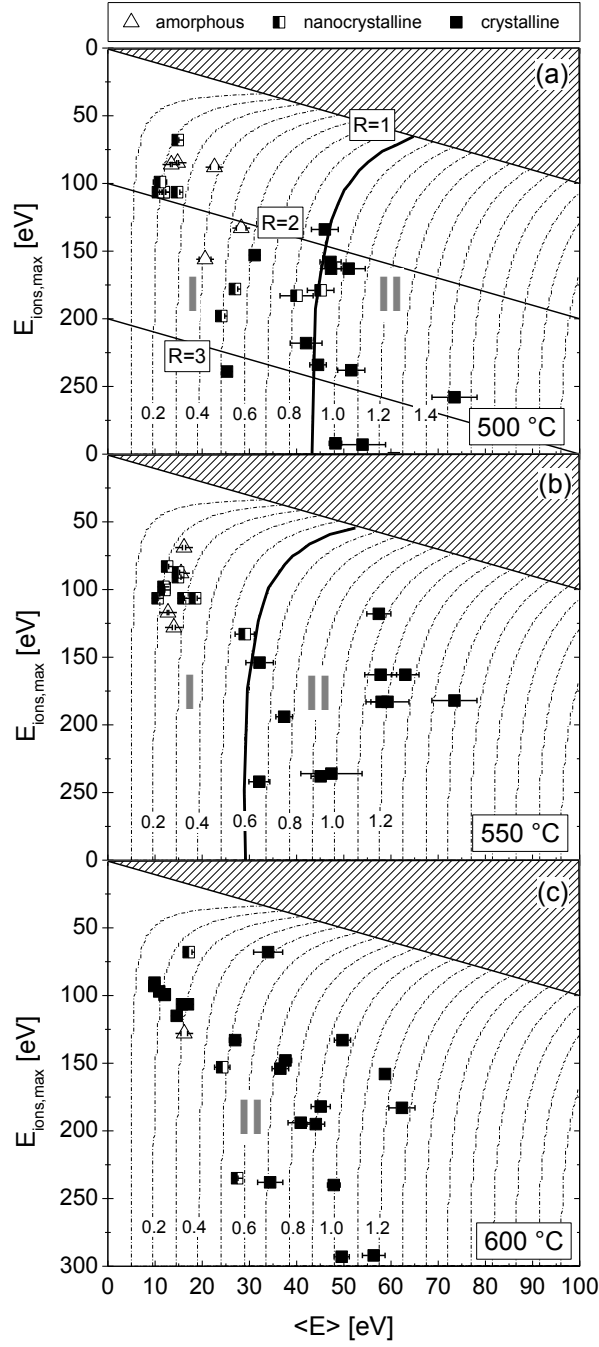


FIG. 4. Al_2O_3 film structure as identified from the XRD- and FTIR spectra being amorphous (open triangles), nanocrystalline (half filled squares), or crystalline (filled squares) in dependence on the average energy per incorporated atom $\langle E \rangle$ and the maximum ion energy $E_{ions,max}$. The shaded areas exclude unreasonable combinations of $\langle E \rangle$ and $E_{ions,max}$. The substrate temperature during deposition was set at 500 °C (a), at 550 °C (b), or at 600 °C. The contour lines show the displacements per atom (dpa), as calculated from the displacements per ions (dpi) simulated by TRIM and the ion-to-neutral ratio in the growth flux. The measured film structures are separated into two regions I and II, characterized by different dpa levels. The ion flux to total growth flux ratio R is shown as straight lines in (a).

The resulting dpa levels are then plotted as contour lines in Figure 4, separating the samples into two regions (indicated as I and II in Figure 4) for different substrate temperatures:

- **Deposition at 500°C:** in region I ($\text{dpa} < 0.9$), most films are amorphous or nanocrystalline, while in region II ($\text{dpa} > 0.9$) all films are crystalline. The threshold may also be aligned to a certain mean energy per deposited atom $\langle E \rangle$, which might be detected at 43 eV.

The observation of different dpa threshold values being necessary for a structural transformation from amorphous to nanocrystalline or from nanocrystalline to amorphous, respectively, is consistent with the current understanding of energetic film formation: a certain energy input is required to allow for the formation of a specific phase of the material.

The separation of the samples into different regions depending on the dpa level is similar to a criterion solely based on the average energy per deposited atoms for ion energies above 150 eV. This is illustrated by the contour lines being almost parallel to the y-axis due to the linear relationship between dpa and ion energy at high energies (see Figure 3).

The separation of the samples into different regions may be regarded in more detail. Petrov *et al.*⁷ made an observation indicating that besides an average energy, the absolute energy has to be at least high enough for the incident ion to penetrate into the material and to displace atoms. This criterion, however, is already the basis of the dpa contour plots. In our case, we still see structural changes although the dpa level remains the same if we follow individual contour lines at the border between the regions. The only remaining difference for those samples is the fact that the dissipated energy is distributed among several species for $E_{ions,max} > 200$ eV, but dissipated only by a few atoms for $E_{ions,max} < 150$ eV. The number of atoms that dissipate the ion energies are given by the flux ratios, which are additionally plotted in Figure 4 (a).

- **Deposition at 550°C:** in region I ($\text{dpa} < 0.6$) most films are amorphous or nanocrystalline, while above a dpa value of 0.6 all films become crystalline. One can clearly see that the boundaries between amorphous or nanocrystalline films to crystalline films shifts to lower dpa levels. This is consistent with the current understanding of film formation that less ion-induced mobility is required at higher substrate temperatures.

- **Deposition at 600°C:** all films become crystalline, irrespective of the dpa level. Apparently, the substrate temperature is high enough so that even very small dpa levels are already sufficient to induce the formation of crystalline films. A clear transition between region II and I cannot be identified anymore in our data set.

A close inspection of Figure 4 shows that very few samples are not located consistently in the respective region - crystalline films in region I instead of II, or amorphous/ nanocrystalline films in region II instead of I. This deviation may be induced by two effects, the variation in the nucleation process or the variation in the grain size distribution:

- (a) In nucleation a delicate competition between amorphous and crystalline phases can occur, where small deviations in the initial condition such as substrate morphology, contamination etc. may lead to growth of completely different film structures.
- (b) The distinction between crystalline and amorphous films by XRD depends very sensitive on the grain size distribution. For small grains or low grain size density, a crystalline phase might easily be undetected by XRD. However, it should be emphasized that the vast majority of samples can consistently be located in region I and II, respectively.

The mapping of the film structure on the parameters of the energy input during film growth expressed in $E_{ions,max}$ and $\langle E \rangle$ and its comparison to the dpa levels that are induced during film growth shows good agreement. One may extrapolate this scaling to Al_2O_3 deposition in general, to predict the film structure in the plasma based on the operating parameters of the system. The description of the IEDF with a maximum ion energy is only reasonable for rectangular bias. The underlying important quantity however is the dpa level in the film, which can be uniquely calculated using TRIM calculations for any ion energy distribution function. The extrapolation of the proposed scaling approach for other bias waveforms is currently under way.

IV. CONCLUSION

Al_2O_3 thin films have been deposited at substrate temperatures between 500°C and 600°C by reactive magnetron sputtering using an additional arbitrary substrate bias to tailor the energy distribution of the incident ions. The formation of crystalline films as opposed to amorphous or nanocrystalline films depends on a critical threshold of 0.9 displacement per incorporated atom at 500°C substrate temperature. This threshold shifts to 0.6 dpa with increasing substrate temperature to 550°C . One can conclude that for fixed neutral to ion fluxes to the film surface, the dpa value is a predictor for the formation of crystalline Al_2O_3 films. The driving mechanism of the formation of crystalline structures is the enhanced mobility of surface atoms due to Ar ion bombardment. As the dpa value increases, the formation temperature of crystalline Al_2O_3 thin films is decreased.

V. ACKNOWLEDGMENT

The authors would like to thank Norbert Grabkowski for his technical support within the experimental setup.

This project is supported by DFG (German Research Foundation) within the framework of the Special Research Field SFB-TR 87 and the Research Department ‘Plasmas with Complex Interactions’ at Ruhr-Universitt Bochum.

Finally, the authors like to thank M. Shihab and R.P. Brinkmann for their support in modeling the ion energy distribution functions for a given bias signal at the electrodes.

REFERENCES

- ¹K. Koski, J. Hölsä, and P. Juliet, *Thin Solid Films* **339**, 240 (1999), ISSN 00406090, URL <http://linkinghub.elsevier.com/retrieve/pii/S0040609098012322>.
- ²P. J. Clarke, *Journal of Vacuum Science & Technology A: Vacuum, Surfaces, and Films* **12**, 594 (1994), ISSN 07342101, URL <http://link.aip.org/link/?JVA/12/594/1&Agg=doi>.
- ³E. Wallin, T. I. Selinder, M. Elfving, and U. Helmersson, *EPL (Europhysics Letters)* **82**, 36002 (2008), ISSN 0295-5075, URL <http://stacks.iop.org/0295-5075/82/i=3/a=36002?key=crossref.fada472bbee68e1835daeba98887bc9a>.
- ⁴O. Zywitzki, G. Hoetzsch, F. Fietzke, and K. Goedicke, *Surface and Coatings Technology* **82**, 169 (1996), ISSN 02578972, URL <http://linkinghub.elsevier.com/retrieve/pii/0257897295002707>.
- ⁵J. Rosén, J. M. Schneider, and K. Larsson, *Solid State Communications* **135**, 90 (2005), ISSN 00381098, URL <http://linkinghub.elsevier.com/retrieve/pii/S0038109805003078>.
- ⁶J. Rosén, S. Mráz, U. Kreissig, D. Music, and J. M. Schneider, *Plasma Chemistry and Plasma Processing* **25**, 303 (2005), ISSN 0272-4324, URL <http://www.springerlink.com/index/10.1007/s11090-004-3130-y>.
- ⁷F. Adibi, I. Petrov, J. E. Greene, L. Hultman, and J.-E. Sundgren, *Journal of Applied Physics* **73**, 8580 (1993), ISSN 00218979, URL http://jap.aip.org/resource/1/japiau/v73/i12/p8580_s1http://link.aip.org/link/JAPIAU/v73/i12/p8580/s1&Agg=doi.
- ⁸I. Petrov, F. Adibi, J. E. Greene, L. Hultman, and J.-E. Sundgren, *Applied Physics Letters* **63**, 36 (1993), ISSN 00036951, URL http://apl.aip.org/resource/1/applab/v63/i1/p36_s1http://link.aip.org/link/APPLAB/v63/i1/p36/s1&Agg=doi.
- ⁹J. Musil, S. Kadlec, V. Valvoda, R. Kužel, and R. Černý, *Surface and Coatings Technology* **43-44**, 259 (1990), ISSN 02578972, URL <http://linkinghub.elsevier.com/retrieve/pii/025789729090079R>.
- ¹⁰V. Poulek, J. Musil, R. Černý, and R. Kuzel, *Thin Solid Films* **170**, L55 (1989), ISSN 00406090, URL <http://linkinghub.elsevier.com/retrieve/pii/0040609089907384>.
- ¹¹V. Poulek, J. Musil, V. Valvoda, and R. Kuzel, *Thin Solid Films* **196**, 265 (1991), ISSN 00406090, URL <http://linkinghub.elsevier.com/retrieve/pii/004060909190370D>.

- ¹²G. Grigorov, I. Martev, M. Stoyanova, J.-L. Vignes, and J.-P. Langeron, *Thin Solid Films* **198**, 169 (1991), ISSN 00406090, URL <http://linkinghub.elsevier.com/retrieve/pii/004060909190335U>.
- ¹³M. Prenzel, A. Kortmann, A. von Keudell, F. Nahif, J. M. Schneider, M. Shihab, and R. P. Brinkmann, *Journal of Physics D: Applied Physics* **46**, 084004 (2013), ISSN 0022-3727, URL <http://stacks.iop.org/0022-3727/46/i=8/a=084004?key=crossref.3977466fb5377ee9197df775317007f8>.
- ¹⁴M. Gautier, G. Fenaud, L. Pham Van, B. Villette, M. Pollak, N. Thromat, F. Jollet, and J.-p. Duraud, *Journal of the American Ceramic Society* **77**, 323 (1994), ISSN 0002-7820, URL <http://doi.wiley.com/10.1111/j.1151-2916.1994.tb06999.x>.
- ¹⁵K. Jiang, K. Sarakinos, S. Konstantinidis, and J. M. Schneider, *Journal of Physics D: Applied Physics* **43**, 325202 (2010), ISSN 0022-3727.
- ¹⁶K. Sarakinos, D. Music, F. Nahif, K. Jiang, a. Braun, C. Zilkens, and J. M. Schneider, *physica status solidi (RRL) - Rapid Research Letters* **4**, 154 (2010), ISSN 18626254, URL <http://doi.wiley.com/10.1002/pssr.201004133>.
- ¹⁷D. Music, F. Nahif, K. Sarakinos, N. Friederichsen, and J. M. Schneider, *Applied Physics Letters* **98**, 111908 (2011), ISSN 00036951, URL <http://link.aip.org/link/APPLAB/v98/i11/p111908/s1&Agg=doi>.
- ¹⁸J. Rosen, E. Widenkvist, K. Larsson, U. Kreissig, S. Mraz, C. Martinez, D. Music, and J. M. Schneider, *Applied Physics Letters* **88**, 191905 (2006), ISSN 00036951, URL <http://link.aip.org/link/APPLAB/v88/i19/p191905/s1&Agg=doi>.
- ¹⁹J. M. Schneider, B. Hjorvarsson, X. Wang, and L. Hultman, *Applied Physics Letters* **75**, 3476 (1999), ISSN 00036951, URL <http://link.aip.org/link/APPLAB/v75/i22/p3476/s1&Agg=doi>.
- ²⁰G. M. W. Kroesen, G. S. Oehrlein, and T. D. Bestwick, *Journal of Applied Physics* **69**, 3390 (1991), ISSN 00218979, URL <http://link.aip.org/link/JAPIAU/v69/i5/p3390/s1&Agg=doi>.
- ²¹M. Shihab, D. Ziegler, and R. P. Brinkmann, *Journal of Physics D: Applied Physics* **45**, 185202 (2012), ISSN 0022-3727, URL <http://stacks.iop.org/0022-3727/45/i=18/a=185202?key=crossref.32271c08a9a890ec429db0cee1751d5b>.
- ²²I. Levin and D. Brandon, *Journal of the American Ceramic Society* **81**, 1995 (1998), ISSN 00027820, URL <http://dx.doi.org/10.1111/j.1151-2916.1998.tb02581.x><http://>

doi.wiley.com/10.1111/j.1151-2916.1998.tb02581.x.

- ²³M. Prenzel, A. Kortmann, A. von Keudell, F. Nahif, J. M. Schneider, M. Shihab, and R. P. Brinkmann, *Journal of Physics D: Applied Physics* **46**, 084004 (2013), ISSN 0022-3727, URL <http://stacks.iop.org/0022-3727/46/i=8/a=084004?key=crossref.3977466fb5377ee9197df775317007f8>.
- ²⁴P. Bruesch, R. Koetz, H. Neff, and L. Pietronero, *Physical Review B* **29**, 4691 (1984).
- ²⁵Y. T. Chu, J. B. Bates, C. W. White, and G. C. Farlow, *Journal of Applied Physics* **64**, 3727 (1988), ISSN 00218979, URL http://jap.aip.org/resource/1/japiau/v64/i7/p3727_s1http://link.aip.org/link/JAPIAU/v64/i7/p3727/s1&Agg=doi.
- ²⁶W. Möller and W. Eckstein, *Nuclear Instruments and Methods in Physics Research Section B: Beam Interactions with Materials and Atoms* **2**, 814 (1984), ISSN 0168583X, URL <http://linkinghub.elsevier.com/retrieve/pii/0168583X84903215>.